

Numerical Study on Suppression of Vortex Induced Vibration of Box Girder Bridge Section by Aerodynamic Countermeasures

Muhammad Waheed SARWAR^a, Takeshi ISHIHARA^b & Yozo FUJINO^c

^{a,b}*Institute of Engineering Innovation, School of Engineering, The University of Tokyo, Japan*
^c*Department of Civil Engineering, The University of Tokyo, Tokyo, Japan*

ABSTRACT: In this study, aerodynamic vibration control measures are used to investigate the suppression mechanism of vortex-induced vibration for box girder bridge section using three-dimensional LES turbulence model. Flow around box girder section with different aerodynamic measures is analyzed and effect of these measures on the aerodynamic characteristics of bridge section is evaluated. Forced vibration is simulated in order to examine the aeroelastic characteristics of bridge section and attention is focused on frequency response component of unsteady lift forces. The response of bridge section with aerodynamic countermeasures is investigated by conducting free vibration simulation, and predicted amplitude of vibration is compared with experimental results. Flow visualization is employed to examine change in flow conditions around bridge section. Further, a method is proposed, based on identification of critical reduced velocity, to efficiently predict maximum amplitude of vibration.

KEYWORDS: Vortex induced vibrations, Aerodynamic measures, Box girder bridge, LES

1 INTRODUCTION

Safety of long span bridges against wind loads is being of primary concern during design process. The interaction of wind and small vibrations of bridge girder leads to wind loads that result in violent motion of bridge girders. Wind-induced phenomena, particularly vortex-induced vibrations (VIV) are often critical for safety and serviceability of long span bridges [1].

Since selection of basic shape for bridge deck depends on many affairs such as structural and economical advantages. The basic deck shape does not necessarily have optimal aerodynamic efficiency. As a consequence, long span bridges are often subjected to vortex induced vibrations, examples of which are Trans-Tokyo Bay Bridge and Storebælt Suspension Bridge. Different types of aerodynamic measures (ADM) are often tested experimentally to obtain suitable vibration control measures [2]. However, testing of such measures are done on case-by-case basis e.g., fairing (F), double flap (DF) and skirt (S) were examined for Trans-Tokyo Bay Bridge [3] and guide vanes were found suitable for Storebælt Suspension Bridge [4]. Efficiency of such measures is found dependent on the geometrical configuration of bridge sections [2]. Therefore, a measure suitable for one bridge section may show adverse effects in another case [5]. In addition, these studies lack information on vibration suppression mechanism of such measures and don't provide any guidance to select countermeasure for bridges experiencing similar problem.

Recently, some works have shown prediction of vortex-induced vibrations using different numerical methods [6-9]. However, in these studies, section attachments were ignored due to modeling difficulty involved because of their smaller size that are as small as 1:100 of section depth. At present, inclusion of aerodynamic countermeasures is highly desirable to investigate the influence of such measures on flow around bridge sections and to clarify the mechanism of

vibration control. So that a general guideline for selection of aerodynamic countermeasure could be established.

This study aims to provide a comprehensive investigation in order to clarify the mechanism of reduction in amplitude of VIV by ADMs for Box Girder Bridge using LES approach. First the aeroelastic instability of rectangular prism with aspect ratio equivalent to that of bridge section is investigated. Then, influence of aerodynamic measures on unsteady aerodynamic characteristics of bridge section is analyzed, and a method is proposed to efficiently predict maximum amplitude of vibration using numerical simulation. Finally, flow visualization is employed to examine modifications done to flow around bridge section by aerodynamic countermeasures.

2 NUMERICAL MODEL

LES turbulent model is used for this study in which small eddies are modeled whereas large eddies are directly calculated. Capability of LES model to capture turbulence characteristics that are unsteady and three dimensional in nature makes it the most suitable approach for this study.

2.1 Governing Equations

The governing equations employed for LES are obtained by filtering the time-dependent Navier-Stokes equations as follows:

$$\frac{\partial \bar{\rho} \bar{u}_i}{\partial x_i} = 0; \quad \frac{\partial}{\partial t} (\bar{\rho} \bar{u}_i) + \frac{\partial}{\partial x_j} (\bar{\rho} \bar{u}_i \bar{u}_j) = \frac{\partial}{\partial x_j} \left(\mu \frac{\partial \bar{u}_i}{\partial x_j} \right) - \frac{\partial \bar{p}}{\partial x_i} - \frac{\partial \tau_{ij}}{\partial x_j} \quad (1)$$

where \bar{u}_i , \bar{p} and $\bar{\rho}$ are filtered mean velocity, filtered pressure and air density respectively. τ_{ij} is sub grid-scale stress resulting from the filtering operation are unknown, and modeled as follows:

$$\tau_{ij} = -2\mu_t \bar{S}_{ij} + \frac{1}{3} \tau_{kk} \delta_{ij}; \quad \bar{S}_{ij} = \frac{1}{2} \left(\frac{\partial \bar{u}_i}{\partial x_j} + \frac{\partial \bar{u}_j}{\partial x_i} \right) \quad (2)$$

where μ_t is the subgrid-scale turbulent viscosity, and \bar{S}_{ij} is the rate-of-strain tensor.

2.2 Smagorinsky-Lilly model

The subgrid-scale turbulent viscosity μ_t is modeled using Smagorinsky model. In this model, the eddy-viscosity is modeled as:

$$\mu_t = \rho L_s^2 |\bar{S}| = \rho L_s \sqrt{2\bar{S}_{ij}\bar{S}_{ij}}; \quad L_s = \min(k\delta, C_s V^{1/3}) \quad (3)$$

where L_s is the mixing length for subgrid-scales and k is the von Kármán constant, C_s is the Smagorinsky constant, δ is the distance to the closest wall, and V is the volume of the computational cell.

2.3 Description of modeling domain

The computational domain used in this study for both rectangular prism (B/D=4) and box girder bridge section (B/D=3.84) with different countermeasures is shown in Fig. 1. An enlarged view of the geometrical configuration and meshing in vicinity of counter measures are summarized in Fig. 2. Mesh elements of large sizes are used in the inlet zone, outlet zone and the domain area far from the bridge section. Fine grid is used only in the region closer to bridge section. Since

section attachments are smaller in size compared to section dimensions, and it would require more number of grid meshes to capture the flow accurately. Therefore, domain is further divided into several zones to deal with the complexity of geometry as shown in Fig. 2d. Use of such sub-domains not only helps to generate reasonable meshing but also allow use of less number of mesh with sufficient accuracy to speed up the calculation process.

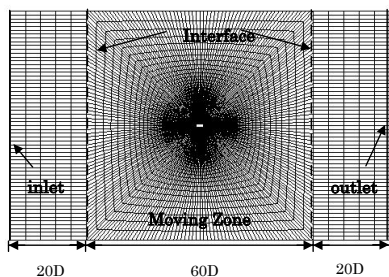


Figure 1. Overview of computational domain

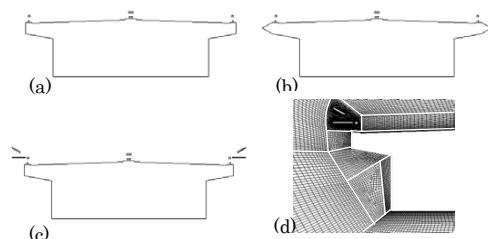


Figure 2. Geometry of section a) Sec, b) Sec+ F, c) Sec+DF and d) mesh around complex geometry of Sec+DF

2.4 Numerical Conditions

Model sections are subjected to oscillations in the heaving mode only. A sliding mesh technique with non-periodic grid interface is employed to allow forced/free oscillations of sections in vertical direction. The boundary conditions for wall zones are specified as no-slip. For both forced and free vibration analysis, symmetry conditions were used for top and bottom surface of domain, and there is zero-convective flux and zero-diffusive flux in the span wise direction. Whereas velocity inlet conditions are employed at the upper and lower boundaries to keep smooth flow in far regions. In addition, boundary conditions for wall zones resulting from interface faces are set to be velocity-inlet.

Unstructured finite volume method using collocated grid was used for the analysis purposes. A sensitivity study was carried out to obtain optimum under-relaxation coefficients (URC) that are found as 0.9 and 0.9 for pressure and velocity respectively. Central difference scheme for convective term and the second order implicit scheme for unsteady term were used to discretize basic algebraic equations. SIMPLE method was used to solve the algebraic equations. The analysis and geometrical conditions of prism and bridge section models are summarized in Table 1.

Table 1. Model dimensions and analysis conditions for prism and Trans-Tokyo Bay Bridge

	Units	Prism	Bridge Section
Width (B)	[m]	0.04	0.0381
Depth (D) at mid-span	[m]	0.01	0.01
Spanwise length (L)	[m]	0.015	0.01
B/D		4.0	3.81
Reynolds Number		1.3×10^4	1.0×10^4
Wind velocity	[m/s]	20	20
Area A (L×D)	[m ²]	0.00015	0.000382
Non-dimensional time step ($\Delta tU/D$)		0.04	0.053
Time step (Δt)	[sec]	2.0e-5	2.667E-05

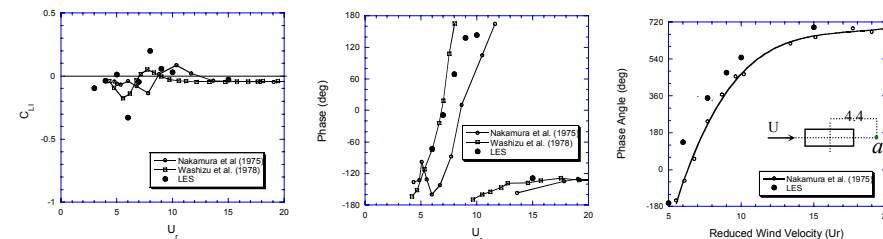
3 RESULTS AND DISCUSSION

This section discusses the frequency response component (FRC) of unsteady lift force and the suppression mechanism of vortex-induced vibrations (VIV) by ADM. The characteristic of wake flow is examined by evaluating the phase difference of wake velocity and oscillation amplitude. Also variation of pressure around bridge sections is visualized to examine the influence of ADM on flow characteristics that resulted in reduced amplitude of vibrations.

3.1 Frequency response components of unsteady lift and wake velocity for rectangular section

The investigations on aeroelastic instability of rectangular prism of width to depth ratio of 4 are summarized in this section. Previous experimental study [10] has shown that large oscillatory amplitude results only in positive aerodynamic damping. Whereas at small amplitude of vibration, FRC of C_L results in negative aerodynamic damping [10]. Therefore, an oscillatory amplitude of 0.02D is used in this study to predict the aerodynamic instability of model section.

Fig. 3 exhibits the characteristic frequency response (FR) of rectangular prism subjected to forced oscillation of amplitude 0.02D. The ordinates are dimensionless lift force component (C_{L1}) and phase angle (β), whereas the abscissa is the reduced wind velocity ($U_r=U/fD$). The variation of imaginary part of lift coefficient corresponding to the instability caused by the negative aerodynamic damping can be seen in Fig. 3a. C_{L1} has shown change from negative to a positive value at lower reduced velocity of 8, and again attained negative sign for higher reduced velocity range. Thus, indicating the presence of self excited vibration at about $U_r=8$, called vortex induced vibrations. Also a change in sign of C_{L1} (from -ve to +ve value) at $U_r=5$ is obtained from numerical results that is in accordance with the pattern observed from experimental outcomes [10,11]. The tendency of C_{L1} to remain negative, at higher reduced velocities, represents absence of galloping for the section that is in accordance with the experimental findings. In addition, an abrupt change in the phase of lift and amplitude of vibration is observed near the critical reduced velocity as shown in Fig. 3b. A good agreement is found between the current simulation results and experimental results [10,11] regarding the onset of instability at low reduced velocities.



a) Imaginary part of unsteady lift
Figure 3. FR components of unsteady lift force acting on section B/D=4

b) Phase of unsteady lift
Figure 4. Phase angle (β) of FR component for wake flow velocity

Fig 4 illustrates the change in phase angles of frequency response component of the wake flow velocity $U_w(t)$ with increase in reduced velocity. The wake flow velocity vibrations was measured at the point "a" shown in the Fig 4. The measurement point was kept stationary to match the experimental setup. The procedure used to calculate the frequency response is similar to that used for the unsteady lift force coefficient. Tendency of sharp increase in phase angle at low reduced velocities can be observed in Fig 4. However, a mild change in phase angle is ob-

tained at higher reduced velocities. At low reduced velocity, fairly close resemblance can be observed, and small difference might be caused by setup inconsistency. A good agreement between the simulated phase angle of wake velocity and experimental results [11] demonstrates the capability of LES model for the wake flow investigations.

3.2 Unsteady lift force in presence of aerodynamic countermeasures

Forced oscillation simulations were carried out by subjecting moving region to sinusoidal amplitude at desired frequency. The amplitude of oscillation was kept 0.02D for all cases. In addition, to avoid any effect arising from change in Reynolds number, oscillatory frequency is changed to increase the reduced velocity, rather than changing velocity of wind flow that is usual way in wind tunnel experiments. The unsteady lift history is decomposed using frequency response analysis (FR) into real (C_{LR}) and imaginary (C_{LI}) components that corresponds to negative aerodynamic damping. Then lift component (C) represents the FRC that corresponds to occurrence of VIV. Fig 5(a,b) shows that negative aerodynamic damping occurs for bridge section with and w/o fairings, and a spike is observed for C. Whereas, use of double flap did not show such spike for C, but has resulted in a small negative aerodynamic damping (Fig 5c). This decrease in FRC with different ADM also indicates the severity of the instability caused by vortex induced vibrations.

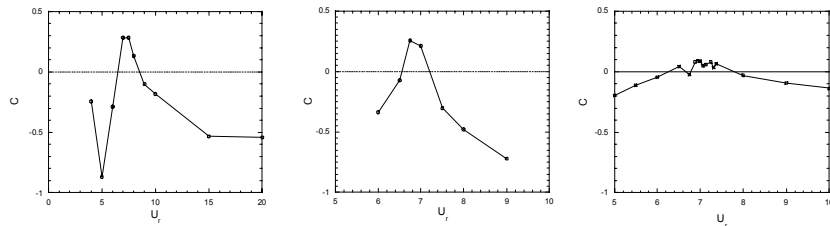


Figure 5 Variation of unsteady lift components with reduced velocity for various bridge sections

In wind tunnel experiments, determination of critical velocity corresponding to maximum amplitude of vibration is obtained by performing free vibration experiments over a range of reduced velocity. However, in numerical testing, this method would be very cumbersome and expensive. Therefore, use of forced vibration is proposed to identify critical reduced velocity. In this method, reduced velocity corresponding to maximum negative aerodynamic damping, obtained by FRC of unsteady lift force [10], would be identified as U_{cr} and further analysis is carried out employing the proposed method. A schematic flow chart of proposed method is shown in Fig 5.

To ascertain the efficiency of the proposed method for determining the maximum amplitude of vibration, a range of reduced velocity is identified in case of bridge section with/out fairing. The identified ranges are 7 to 7.5, and 6.75 to 7.0 for section w/o fairing and with fairing respectively. However, for the case of section with double flap, an intensive investigation was carried

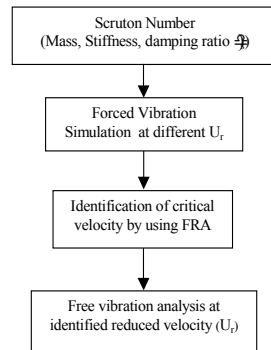


Figure 6. Flow chart to simulate maximum amplitude of VIV

out to accurately identify the critical reduced velocity that turns out to be 6.935. This shows that introduction of ADMs also cause change in critical reduced velocity. Therefore, to determine maximum amplitude of vibration in case of ADMs, it is necessary to check a range in vicinity of critical velocity of section without any measure. Next section describes free vibration simulations that are carried out at the identified critical velocities.

3.3 Reduction in amplitude of vibration by aerodynamic measures

To simulate free vibration cases, fluid structure interaction was employed to evaluate the dynamic response of bridge section under unsteady lift forces. The structural parameters, for free vibration testing, are chosen to ensure that Scruton number is equal to 6 in order to setup conditions equivalent to those of wind tunnel experiments [3].

For the bridge sections with and without fairing, rather large number of free vibration tests was required to obtain the maximum amplitude of vibration within the identified range of reduced velocities. For section only case, maximum amplitude of vibration occurred at $U_r=7.25$ as shown in Fig 7a. For section with fairing (F), large amplitude of vibrations are observed for the identified range of U_r , where maximum amplitude occurs at $U_r=6.82$. Comparison of normalized amplitude history, Fig 7b, shows that even a small change in reduced velocity results in smaller amplitude. However, for bridge section with DF, the identified reduced velocity resulted in maximum amplitude of vibration, which is almost half of amplitude of section with and w/o fairing, as shown in Fig 7c. The use of fairing tends to increase amplitude of vibration, while double flap has helped controlling these vibrations. A good agreement is found among the experimental and numerically predicted amplitude of vibrations as shown in Fig 8.

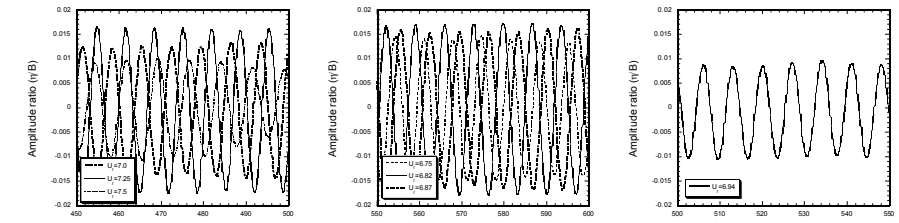


Figure 7. Displacement histories of Bridge Section with and without aerodynamic measures

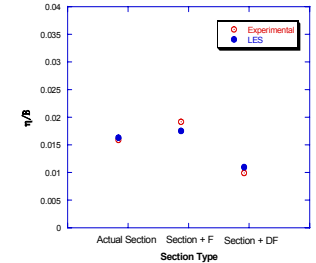


Figure 8. Comparison of maximum amplitude ratio of VIV (Exp [3])

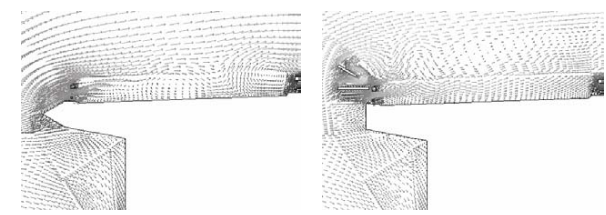


Figure 9. Velocity vectors on the wind ward side of section at $\eta=0$ & $U_r=U_{cr}$

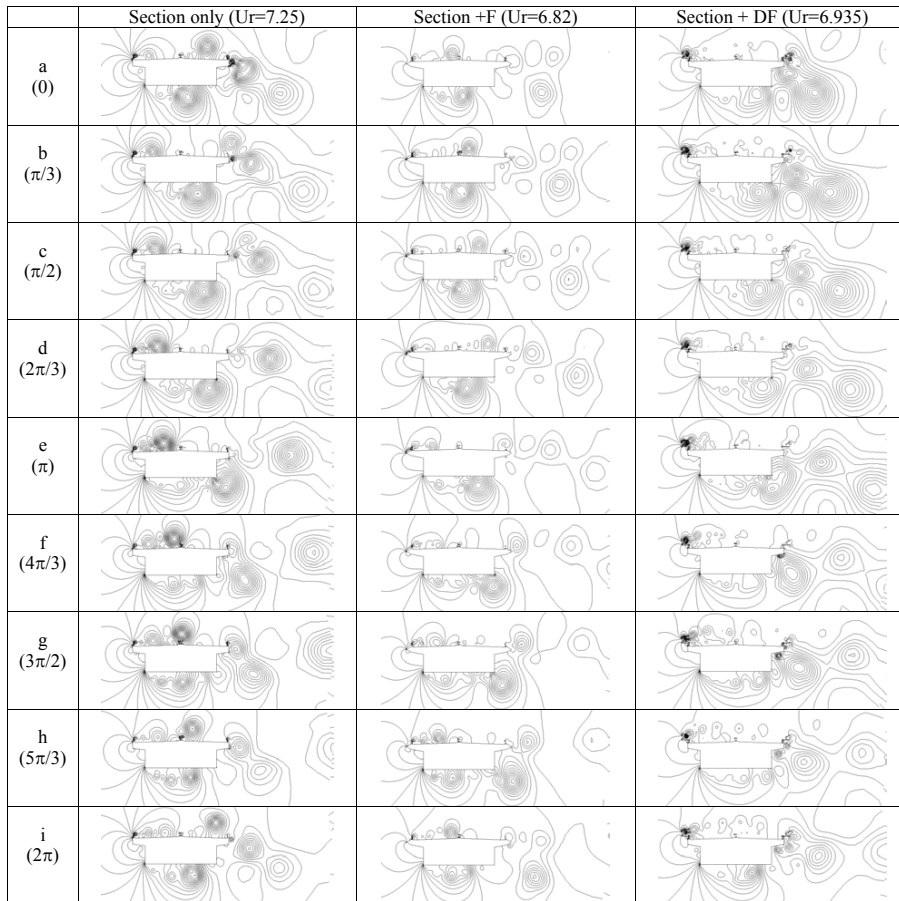


Figure 10. Instantaneous flow patterns for one cycle of free vibration analysis at critical reduced velocities

The reduction of amplitude in presence of double flap can be explained by examining the velocity vectors and pressure distribution around bridge sections with different aerodynamic measures. The wind velocity at the leading edge increases in presence of fairing. Thus intensifying the shear layer, and strong vortex formation is observed on upper surface (Fig 9a). In addition, handrails disturbed the on coming flow, and velocity jet formation between the handrails is observed.

On the other hand, use of double flap has forced flow towards the upper surface and suppresses generation of vortex on the upper surface by disturbing the formation of shear layer. To provide deep insight of this phenomenon, instantaneous pressure distribution of all three cases for one complete oscillatory cycle at respective critical reduced velocities are summarized in Fig 10. In case of bridge section only, vortices are formed on upper and lower surfaces that traveled down to trailing edge, and these vortices are shed alternatively. Thus resulting in large amplitude

of vibration under sinusoidal force. For section with fairing (F), almost similar pattern of vortex shedding is observed (Fig 10) that resulted in a bit larger amplitude of vibration than the original section. On the other hand, in case of section with double flap (DF), vortex formation on lower edge remains undisturbed. However, the strong vortex formation on upper surface has diminished because of disturbance caused to shear layer by the redirected flow of double flap. Instead, small vortices are shed behind DF for the later half of the oscillation ($\pi \sim 2\pi$). Thus, use of double flap resulted in rather smaller oscillatory force acting on the bridge section, which leads to reduced amplitude of vibration.

4 CONCLUSIONS

Vortex induced vibrations and suppression mechanism of box girder bridge section in presence of aerodynamic countermeasures is pursued by means of 3D LES model. The predicted amplitudes of vibration in presence of such small aerodynamic countermeasures are found in very good agreement with those of experimental studies. Flow visualization and pressure distribution has shown that use of double flap caused disturbance to shear layer and generation of strong vortex on upper edge diminishes. However, use of fairing help intensifying the vortex formation on upper surface leading to large amplitude of vibration. From forced vibration testing, aerodynamic measures are found to drastically alter the aerodynamic characteristics of the bridge section. And introduction of double flap results in small negative aerodynamic damping that is basically responsible for vortex induced vibrations. Further, change in critical reduced velocity is observed by the modifications done to basic shape along with the use of aerodynamic countermeasures. In addition, proposed method of identifying critical velocity from forced vibration tests is successfully applied, and it helps reducing computational efforts. Thus making whole process of amplitude prediction more efficient and economical.

REFERENCES

- [1] Sato, H., "Wind resistant design manual for highway bridges in Japan", *J. of Str. Eng.* 91⁽¹²⁻¹⁵⁾ (2003), 1499-1509
- [2] Yoshida, Y., "A study about the vortex induced vibration and control of a continuous steel box girder bridge", *PhD Thesis* (2000), The University of Tokyo.
- [3] "Wind Resistant Design of Bridges—Code Practice and Recent Developments", *Str. Eng. Series 12, JSCE* (2003)
- [4] Larsen, A., Eisdahl, S., et al., "Storebælt suspension bridge – vortex shedding excitation and mitigation by guide vanes", *J. of Wind Eng. Ind. Aerodyn.* 88 (2000), 283-296
- [5] Fujino, Y., Yoshida, Y., "Wind-induced vibration and control of trans-tokyo bay crossing bridge", *J. of Str. Eng.* 128 (2002), 1012-1025
- [6] Frandsen, J.B., "Comparison of numerical prediction and full-scale measurements of vortex induced oscillations", *Proc. of 4th Int. Col. on Bluff Body Aerodyn. & App.* (2000), Germany.
- [7] Frandsen, J. B., "Computational fluid-structure interaction applied to long-span bridges", *PhD Thesis* (1999)
- [8] Sangsan, L., Lee, J. S., and Kim, J. D., "Prediction of vortex-induced wind loading on long-span bridges", *J. of Wind Eng. Ind. Aerodyn.* Vol. 67&68 (1997), 267-278
- [9] Larsen, A., and Walther, J. H., "Aeroelastic analysis of bridge girder sections based on discrete vortex simulations", *J. of Wind Eng. Ind. Aerodyn.* Vol. 67&68 (1997), 253-265
- [10] Washizu, k., Ohya, A., Otsuki, Y. and Fuji, K. (1978) "Aeroelastic instability of rectangular cylinders in a heaving mode", *J. of Sound and Vibration*, 59(2), 195-210
- [11] Nakamura, Y. and Mizota, T. (1975) "Unsteady lifts and wakes of oscillating rectangular prisms". *Journal of the Engineering Mechanics Division*, 885-871